ACS SENSORS

pubs.acs.org/acssensors
Article

Multilayered Bioorthogonal SERS Nanoprobes Selectively Aggregating in Human Fluids: A Smart Optical Assay for β-Amyloid Peptide Quantification

Caterina Dallari, Elena Lenci, Andrea Trabocchi, Valentina Bessi, Silvia Bagnoli, Benedetta Nacmias, Caterina Credi,* and Francesco Saverio Pavone

Cite This: ACS Sens. 2023, 8, 3693−3700
Read Online

ABSTRACT: Alzheimer's disease (AD) is a debilitating neurological condition characterized by cognitive decline, memory loss, and behavioral skill impairment, features that worsen with time. Early diagnosis will likely be the most effective therapy for Alzheimer's disease since it can ensure timely pharmacological treatments that can reduce the irreversible progression and delay the symptoms. Amyloid β-peptide 1−42 (Aβ (1−42)) is considered one of the key pathological AD biomarkers that is present in different biological fluids. However, Aβ (1−42) detection still relies on colorimetric and enzyme-linked immunoassays as the gold standard characterized by low accuracy or high costs, respectively. In this context, optical detection techniques based on surface-enhanced Raman spectroscopy (SERS) through advanced nanoconstructs are promising alternatives for the development of novel rapid and low-cost methods for the targeting of Aβ pathological biomarkers in fluids. Here, a multilayered nanoprobe constituted by bioorthogonal Raman reporters (RRs) embedded within two layers of gold nanoparticles (Au@RRs@AuNPs) has been developed and successfully validated for specific detection of Aβ (1−42) in the human cerebrospinal fluid (CSF) with sensitivity down to pg/mL. The smart double-layer configuration enables us to exploit the outer gold NP surfaces for selective absorption of targeted peptide whose concentration controls the aggregation behavior of Au@RRs@AuNPs, proportionally reflected in Raman intensity changes, providing high specificity and sensitivity and representing a significant step ahead of the state of the art on SERS for clinical analyses.

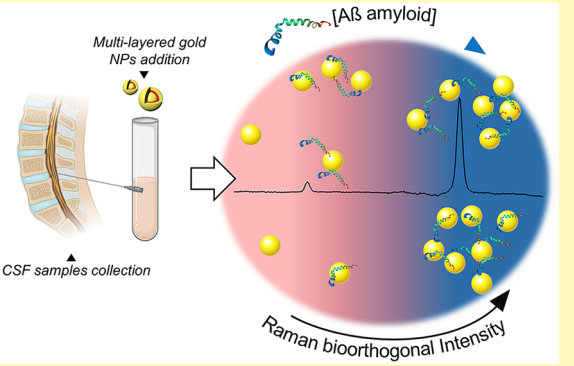

KEYWORDS: *multilayered nanoparticles, SERS-based sensors, bioorthogonal Raman, cerebrospinal fluid, Aβ (1−42) peptides, neurodegenerative biomarker*

Alzheimer's disease (AD) is the leading cause of dementia affecting about 47 million people worldwide. Due to the longer life expectancy, this number is supposed to increase over time with a staggering economic and social impact.[1] It is recognized that the AD pathological hallmarks develop over decades before patients express the initial cognitive changes.[2,3] Therefore, precocious AD diagnosis is crucial to ensure timely treatments that can reduce AD progression and limit the difficulties related to the emotional, physical, and financial aspects of the disease. Current methods for AD diagnosis include immunoassays (IAs) that analyze cerebrospinal fluid (CSF) to target specific biomarkers, whose abnormal concentrations are indicators of AD.[4−6] In this context, the detection of ß-amyloid peptide (Aß) content in CSF is crucial and can provide useful information for the diagnosis of AD and among all, Aß (1−42) peptide is the main factor of toxic amyloid plaque formation, which leads to a loss of cognitive function in AD patients. Despite their sensitivity, conventional IAs require days for test results as well as expensive enzyme-linked antibodies and dedicated expensive laboratory equipment not accessible to every structure.[7−9] Thus, the development of rapid low-cost AD diagnostic tools with improved sensitivity remains an area of intense investigation. In the need to identify an alternative approach, metallic nanoparticles (NPs) have been proven to be attractive and efficient materials for a wide range of biomedical applications both for diagnostics and therapy. In particular, gold NPs (AuNPs) have received enormous attention for the detection of AD biomarkers due to their unique optical properties, biocompatibility, and high surface area, which led to great adsorption capacity on binding

Received: February 7, 2023
Accepted: August 2, 2023
Published: September 27, 2023

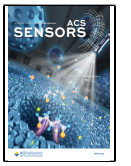

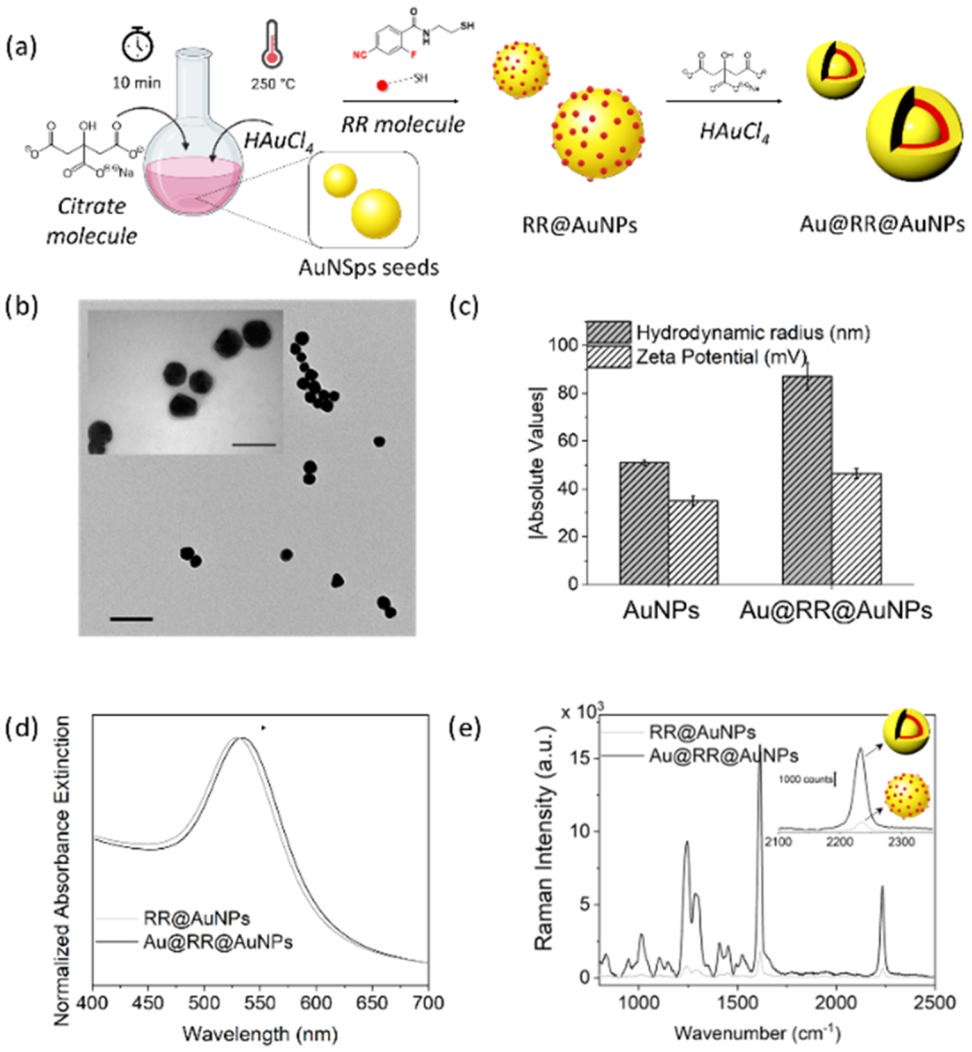

Figure 1. Synthetic strategy implemented for the preparation of RR-embedded double-shell nanoparticles (Au@RR@AuNPs) (a). TEM micrographs of Au@RR@AuNPs; the scale bar is 100 nm. The inset shows a 2× magnification TEM image (scale bar is 50 nm) (b). Size distribution and ζ-potential values for AuNPs and Au@RR@AuNPs (c). UV−vis absorption for RR@AuNPs and Au@RR@AuNPs (d). Raman-SERS spectra of RR@AuNPs and Au@RR@AuNPs. The inset shows the Raman-SERS spectra in the range of 2100−2350 cm^{-1} (e).

the proteins. Indeed, AuNPs can be used simultaneously to modulate Aß aggregation and as sensing elements in optical assays. The study by Zhou et al. reported on the development of a colorimetric-based sensor for the detection of Aβ (1−40) conjugated to AuNPs. They exploited the aggregation induced by Cu^{2+} metal ions, driven by the formation of ternary coordination complexes between the metallic ions and nitrogen and oxygen ligands from Aβ.[10] Yokoyama et al. tested the possibility of self-assembled Aβ (1−42) on spherical AuNPs and investigated the conformational changes using absorption spectroscopy.[11] In these studies, the amyloid β was tested over the range of 7.5−500 nM with limits of detection (LODs) significantly higher with respect to Aβ (1−42) levels in real CSF samples. Therefore, the development of novel strategies is crucial to improve the sensitivity of the NP-based technology, to quantify lower Aβ (1−42) levels and to pave the way for the lab-to-clinic technological transfer. In this direction, detection methods based on surface-enhanced Raman scattering (SERS) through gold NPs represent a powerful approach for revealing target analytes in biological fluids down to fg/mL.[12,13] The surface chemistry of NPs as SERS substrates can be engineered to selectively sense AD biomarkers and to monitor the CSF biochemical changes even in the picomolar range, discriminating between physiological and pathological conditions even for asymptomatic patients. In addition, NP surfaces can be labeled with bioorthogonal Raman reporters (RRs), a novel class of molecules characterized by larger Raman cross sections with respect to biomolecules and narrow peaks in the biological Raman-silent region, ensuring a higher signal-to-noise ratio and drastically decreasing the LOD.[14,15] Therefore, the characteristic peak of these RRs conjugated to the NP surface (RR@AuNPs) that aggregate in the presence of the analytes can be used to indirectly detect the target molecules, taking advantage of changes in Raman intensity due to analyte−RR@AuNPs interactions. Herein, we successfully envisioned to combine the simplicity of aggregation behavior triggered by the target peptide with the high sensitivity of bioorthogonal SERS assays to reveal Aβ (1−42) in clinical human samples down to pg/mL. To this end, we designed and developed extremely efficient SERS nanotags in which the RRs are embedded between a spherical gold core and a protective shell of gold (Au@RRs@AuNPs). In our NP-based assay, we simply exploited the high affinity of Aβ (1−42) toward gold for

https://doi.org/10.1021/acssensors.3c00225
ACS Sens. 2023, 8, 3693−3700

NP−Aβ specific interaction to trigger controlled NP aggregation as a function of analyte concentration. Then, bioorthogonal SERS signal variations were successfully exploited to reveal small changes in Aβ concentration among CSF samples with very small LODs, thus providing a concrete contribution for amyloid-linked pathologies as Alzheimer's disease.

RESULTS AND DISCUSSION

Multilayered Au@RR@AuNPs were realized starting with the synthesis of 50 ± 1 nm diameter gold nanospheres, which serve as cores, followed by immediate exchange of the stabilizing agent (sodium citrate) with a Raman reporter, recently synthesized and characterized by our group.[16] Then, an additional gold shell of desired thickness was grown by adding gold salt ($HAuCl_4$) with citrate ions serving as both capping and mild reducing agents. The volume and the concentration of the RR solution in the ligand exchange step were critical parameters to be adjusted to avoid particle−particle aggregation as well as to achieve full gold surface covering, resulting in a higher Raman signal (Figure S1, Supporting Information). Transmission electron microscopy (TEM) images, reported in Figure 1b, revealed a quite uniform size distribution displaying spherical shape, confirmed by a hydrodynamic diameter distribution of 85 ± 5 nm with a polydispersity index of 0.30 ± 0.02 measured through dynamic light scattering (DLS) measurements (Figure 1c). A ζ-potential value of −45 ± 2 mV further assessed the stability of the colloidal system dispersed in aqueous solution (Figure 1c). Ultraviolet−visible (UV−vis) extinction spectra showed a bathochromic shift of about 5 nm for Au@RR@AuNPs with respect to the original plasmonic peak of RR@AuNPs, confirming a variation in the chemical environment at the NP surface after ligand exchange, which directly affects the extinction coefficient value and therefore the maximum absorbance wavelength (Figure 1d). To further attest the RR embedding, UV−vis measurements acquired at the intermediate step consisting in RR-covered NPs showed the tendency to aggregate in water with the appearance of a red-shifted peak with respect to the starting seeds (Figure S2). Moreover, Raman measurements demonstrated that a 10-times increase of the characteristic Raman peak at 2135 cm^{-1} was obtained for multilayered Au@RR@AuNPs with respect to RR@AuNPs. This could be likely ascribed to the fact that by embedding the Raman emitters molecules within two nanometric layers of gold, the Raman molecules are exposed to enhanced local electromagnetic fields, locally generating "hot spots" at noble metal nanostructure junctions, thus positively strongly impacting the limit of detection of such systems (Figure 1e).

Besides the intrinsic Raman enhancement, the crucial point of this novel SERS sensor is that the outer surface of naked gold NPs could be exploited as substrates to selectively capture the analytes of interest exploiting the high affinity between the Aß (1−42) peptide and gold surfaces. Then, their aggregation was induced by the addition of Cu^{2+} ions (Figure 2). First, UV−vis spectra of Aß (1−42)-decorated NPs were acquired at increasing concentration of metal ions to attest the Cu^{2+}-dependent aggregating behavior. The spectra reported in Figure S3 confirmed that only upon addition of the ions, the plasmonic profile was changed. More interestingly, keeping the Cu^{2+} concentration at 0.48 mM, the plasmonic variation of the colloidal system as a function of β amyloid concentration was

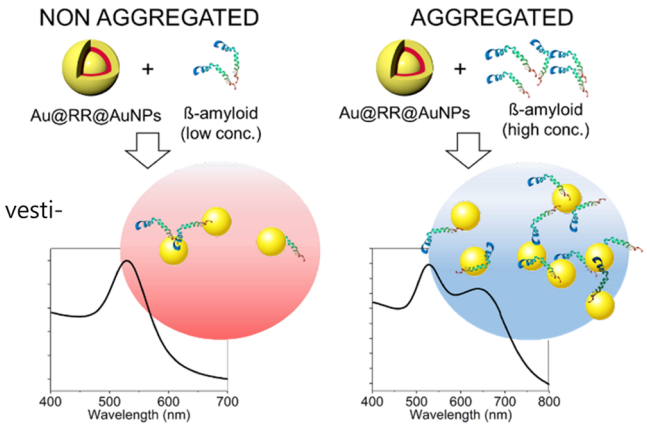

Figure 2. Schematic representation of the aggregation working principle for the developed multilayered gold nanoparticles.

investigated. The pure Au@RR@AuNPs solution was originally stably dispersed due to the electrostatic repulsion of capping-agent molecules, displaying a maximum absorbance value at 524 nm. Upon the addition of Aβ (1−42) proteins together with Cu^{2+} ions, a new strong absorbance peak was observed to rapidly appear at around 680 nm due to the Cu^{2+}-mediated bridging between Aβ-AuNP complexes (Figure 2). Therefore, the red shift was expected to be more pronounced as the quantity of Aβ (1−42) increased due to more Aβ-AuNP complex formation.

We first investigated the possibility to exploit this Aβ-dependent aggregating behavior induced by the complexation of the peptide by Cu^{2+} to set up a UV−vis condition by analyzing the optical spectral changes obtained at varied Au@RR@AuNPs:Aβ(1−42) ratios through three quantitative descriptors (aggregation indexes, AIs), which are deeply explained in the "Aggregation Indexes" Section in the Supporting Information. These were properly defined to be independent, thus guaranteeing neither errors nor generation of false results during data analysis while proving the robustness and fidelity of the adopted method (see Figure 3a−c). Starting from the pure NP solution showing the characteristic 520 peak (blue spectrum), the 680 nm peak was observed to appear and increase until a Aβ (1−42) concentration of about 30 ng/mL (pink curve) as reported in Figure 3d−f. Then, AI values were calculated and plotted (Figure 3g−i). The trend is clearly the same for all three indexes with a linear behavior to Aβ (1−42) concentrations of around 10 ng/mL, thus perfectly working in the detection range considered of clinical interest (Figure 3j−l). The reverse in aggregation behavior observed is probably because when the amount of amyloid monomers is higher than 30 ng/mL (which it is important to highlight that are far from real content in CSF), Aβ (1−42) exceeds a critical aggregation concentration at which it preferentially interacts with the other Aβ (1−42) peptides forming other larger species (e.g., oligomers) that are no more available for Au binding, thus perturbing the colloidal system less. Consequently, the colloidal system tends to retain its optical properties when nonaggregated (with the peak at 680 nm strongly reduced). These results attested that the UV−vis assay based on multilayered Au@RR@AuNPs can be used for the Aβ (1−42) detection in the range of 0.4−30 ng/mL, with a limit of detection (LOD) calculated to be 1.2 ng/mL (0.3 nM), which was lower than that previously reported for colorimetric methods for Aβ (1−42).[10] The 30 ng/mL

https://doi.org/10.1021/acssensors.3c00225
ACS Sens. 2023, 8, 3693−3700

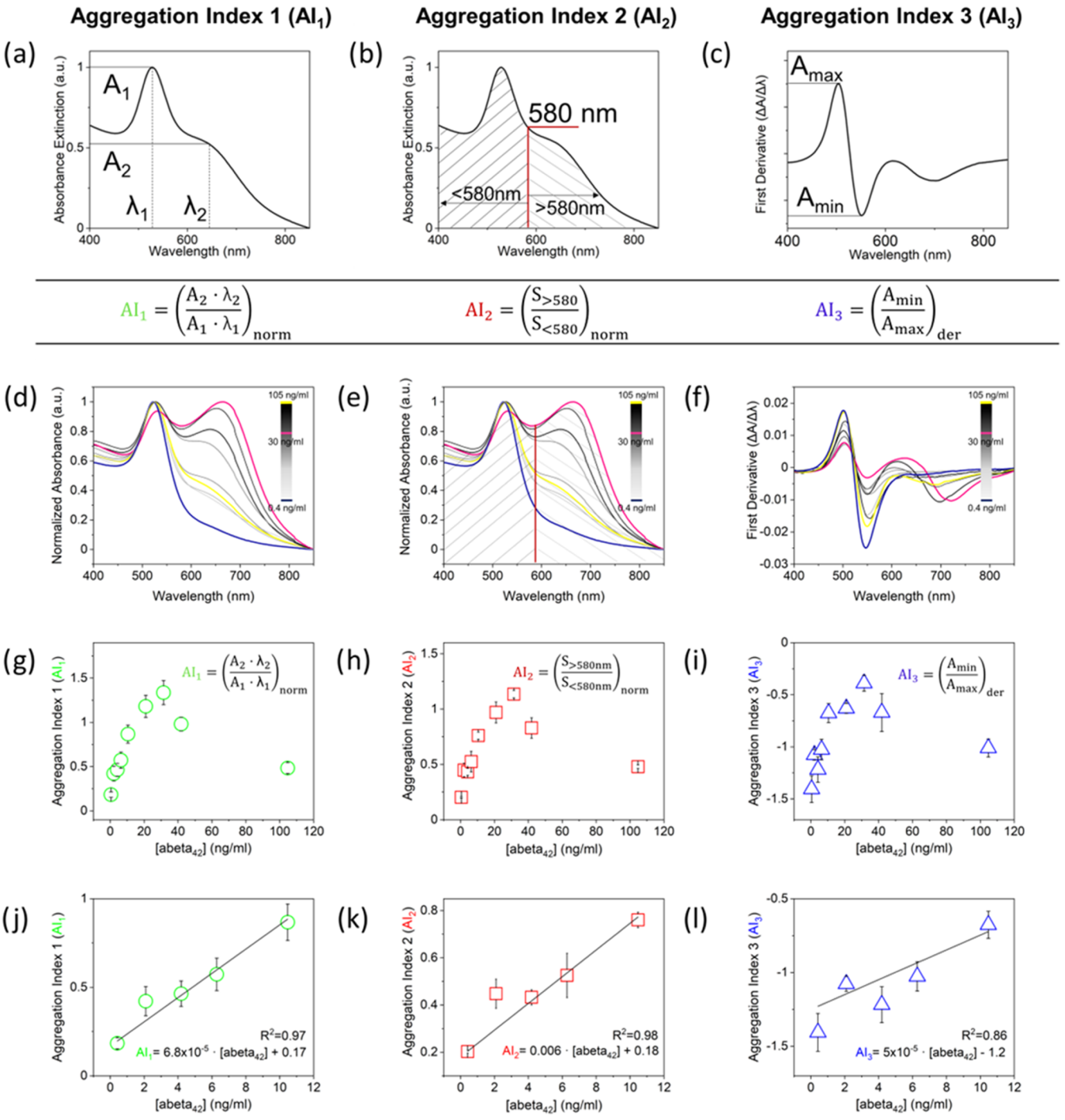

Figure 3. Graphical representation of parameters extracted from the normalized absorbance extinction spectrum for the calculation of aggregation Index 1, AI_1 (a); aggregation index 2, AI_2 (b); graphical representation of parameters extracted from the first derivative spectrum for the calculation of aggregation index 3, AI_3 (c). Table resuming the mathematical calculation for AI_1, AI_2, and AI_3. UV−visible spectra acquired for Au@RR@AuNPs mixed with different quantities of Aβ (1−42) ranging from 0.4 to 105 ng/mL. Spectra are reported normalized to 1 (d, e) and after a first derivative operation (f). Aggregation indexes (AIs) as a function of the Aβ (1−42) concentration calculated from UV−vis data normalized to 1 (g, h) and after a first derivative operation (i). Linear concentration dependence of AIs as a function of the Aβ (1−42) concentration, in the range of 0.4 to 31 ng/mL (j, k, l). (n = 3; error bars represent standard deviation; the black solid line shows linear fitting).

threshold value does not represent a drawback for the potential real application of this method considering that both physiological and pathological Aβ values in real samples are always below 1 ng/mL, as discussed later in the work.

Despite these remarkable findings, considering that real biological fluids are heterogeneous matrices rich in proteins, it was crucial to demonstrate that this "aggregation behavior" is not perturbed by the presence of other proteins at their plausible range in CSF. To this aim, the experiment was replicated by mixing multilayered Au@RR@AuNPs with bovine serum albumin (BSA), a ubiquitous protein present in all biological fluids, at concentrations ranging from 0.4 to 20 ng/mL, and by triggering again the aggregation by adding Cu^{2+} at 0.48 mM concentration. As reported in Figure S4, the trend

https://doi.org/10.1021/acssensors.3c00225
ACS Sens. 2023, 8, 3693−3700

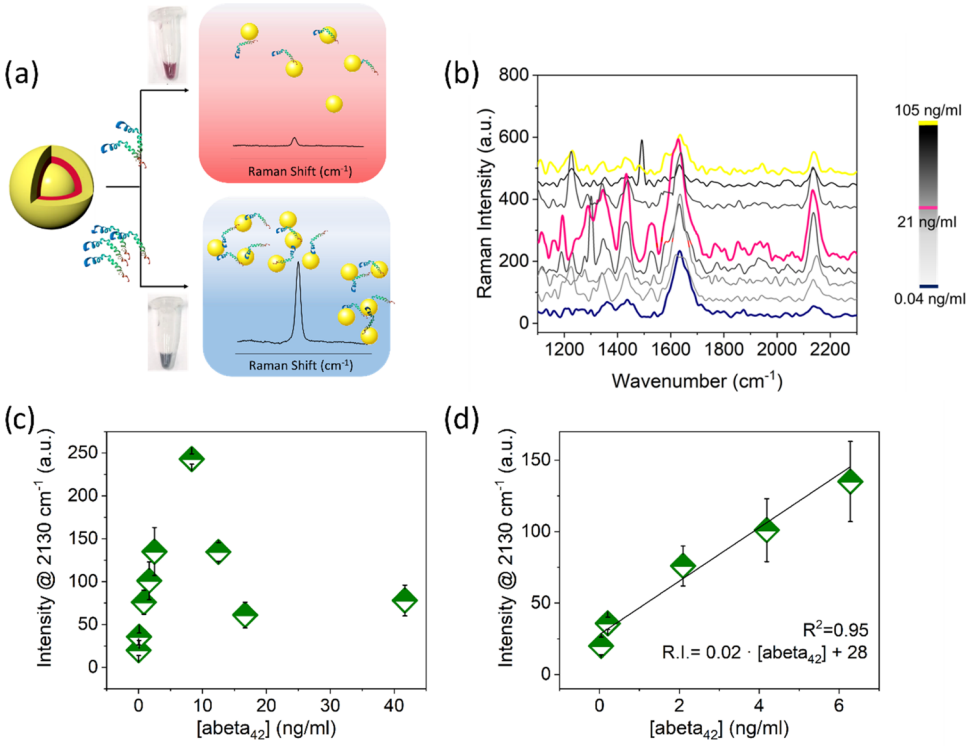

Figure 4. Raman-SERS spectra acquired against Au@RR@AuNPs with different quantities of Aβ (1−42) ranging from 0.04 to 105 ng/mL (a) and plot of the Raman intensity at 2135 cm^{-1} against Aβ (1−42) concentration (b). Linear concentration dependence of Raman intensity as a function of Aβ (1−42) concentration, in the range of 0.04 to 100 ng/mL (c) and 0.04 to 8 ng/mL (d). (n = 4; error bars represent standard deviation; the black solid line shows linear fitting).

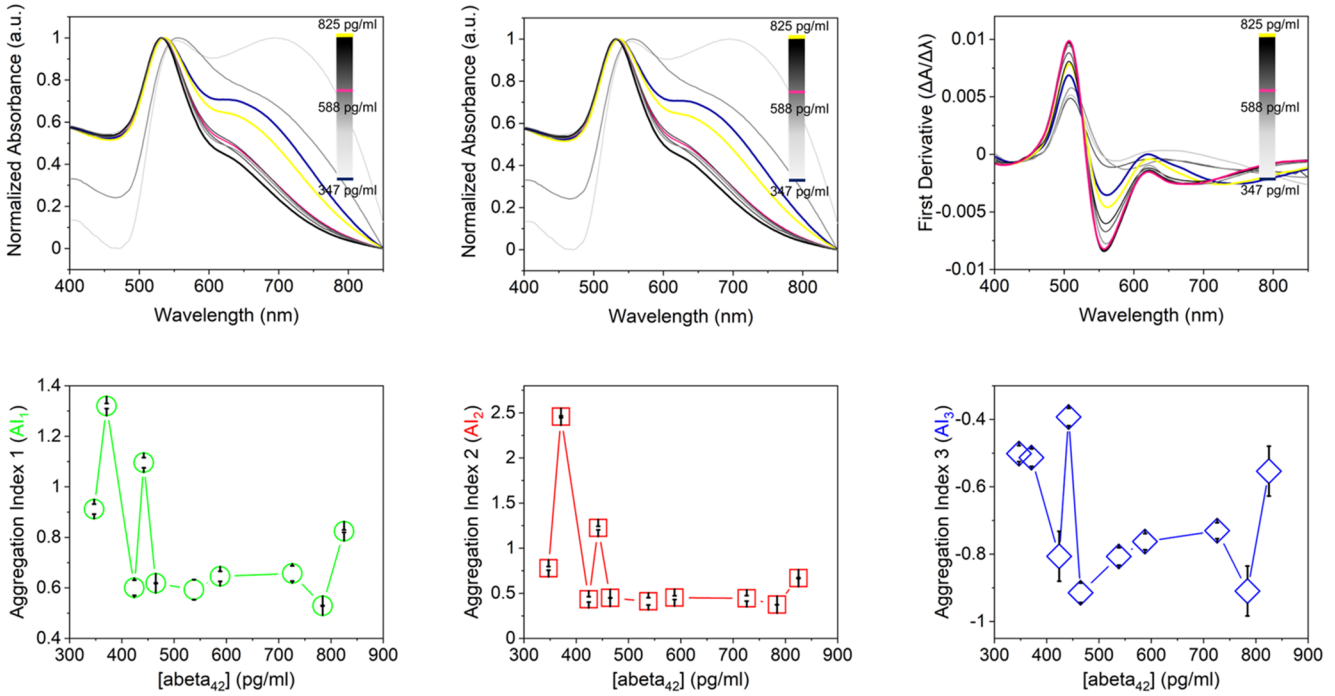

Figure 5. UV−visible spectra acquired for Au@RR@AuNPs mixed with different CSF samples. Spectra are reported raw (a), normalized to 1 (b), and after a first derivative operation (c). Aggregation indexes (AIs) as a function of the Aβ (1−42) concentration in CSF samples calculated from UV−vis data normalized to 1 (d, e) and after a first derivative operation (f). (n = 3; error bars represent standard deviation).

observed for BSA was opposite to that of the peptide, with AI_1 linearly decreasing upon increasing BSA concentration, thus corresponding to poor NP clustering. This could be ascribed to an increase in the stability of the colloids due to the formation of a compact and bulky BSA corona around the NPs that acts as a stabilizing agent, shields the metallic surfaces, and

https://doi.org/10.1021/acssensors.3c00225
ACS Sens. 2023, 8, 3693−3700

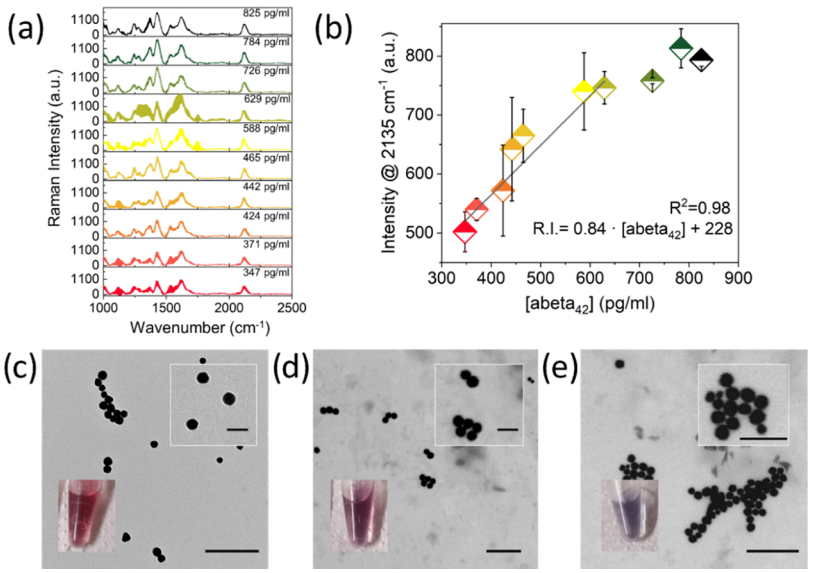

Figure 6. Raman-SERS spectra acquired against Au@RR@AuNPs mixed with different CSF samples with Aβ (1−42) concentrations ranging from 347 to 825 pg/mL (a) and plot of the Raman intensity at 2135 cm^{-1} against the Aβ (1−42) concentration, with linear dependency in the range of 347−629 pg/mL (b). (n = 4; error bars represent standard deviation; the black solid line shows linear fitting). TEM images of different aggregation behaviors of Au@RR@AuNPs for the original colloidal solution (c) and at 347 pg/mL (d) and 629 pg/mL (e) Aβ concentrations. The scale bar is 250 nm in all cases. The inset shows magnified images of the same samples (the scale bar is 100 nm in all cases).

counterbalances the aggregating behavior induced by Cu^{2+} ions desorbing citrate from gold surfaces. In addition, the BSA molecules or albumin-derived molecules typically present in human fluids do not hinder the binding sites for target peptides (Figure S5). These results were fundamental to attest that only with the formation of NP−Aβ complexes, the presence of Cu^{2+} ions induces aggregation, thus pointing out the feasibility to apply the method for the screening of real samples. Before proceeding with this step, SERS response of multilayered aggregating NPs was investigated for Aβ (1−42) quantification by exploiting the intensity values of the Raman peak at 2135 cm^{-1} from RR located in a spectral region completely free from background interferences. The SERS spectra were acquired from colloids after mixing with peptide solution in the 0.04 to 105 ng/mL range (Figure 4a), and it can be found that SERS response increased with increasing Aβ (1−42) peptide. As reported in Figure 4b−d, by plotting the intensity of the RR peak against peptide concentration, a linear trend was observed until about 7 ng/mL with the peak visible down to 0.04 ng/mL (0.01 nM). The LOD of the multilayered SERS system was calculated to be 0.65 ng/ml (10 pM), at least two times lower than the LOD previously obtained with the UV−vis approach. Aβ (1−42) concentrations higher than 30 ng/mL induced the trend inversion as previously observed. To further attest the Aβ (1−42)-dependent aggregation behavior, the synthetic Aβ (1−40) peptide was mixed with multilayered NPs and the aggregation was triggered by Cu^{2+}, following the same experimental procedure implemented for Aβ (1−42). Raman-SERS spectra were acquired for Aβ (1−40) concentrations ranging from 0.5 to 15 ng/mL. As shown in Figure S6, the intensity of the bioorthogonal Raman peak acquired at varied Aβ (1−40) concentrations does not vary significantly, thus demonstrating that there is no direct dependence of Aβ (1−40) peptide concentration on the NP aggregation behavior, triggered by Cu^{2+} ions. As reported from the literature, this could be ascribed to the much lower apparent affinity constant for Aβ (1−40) with Cu^{2+} ions (5.0×10^{-11} M) with respect to the one for Aβ (1−42) with Cu^{2+} (7.0×10^{-18} M).[17,18] This great difference in the way of complexation of the ion probably leads to different aggregation behaviors in terms of time and number of particles interacting.

Finally, the bioorthogonal SERS-based sensor for the detection of Aβ (1−42) based on the Cu^{2+}−AuNP−Ab complex formation was applied and exploited for the quantification of Aβ (1−42) in human CSF. Samples were collected from patients with neurocognitive disorders and previously analyzed by standard fluorescence-based diagnostic kits to quantify Aβ (1−42) and Aβ (1−40), whose values are reported in the table in Figure S7 (values from standard kits were taken as a benchmark). Each CSF sample was mixed with Au@RR@AuNPs and Cu^{2+} to induce Aβ (1−42)-dependent aggregation of the colloidal system, and UV−vis spectra were acquired to determine AIs. However, as shown in Figure 5, no clear trends were observed as a function of peptide concentration. This could be ascribed to the strong dependence of the plasmonic properties of metallic nanoparticles on their size and shape, interparticle distance, number, and disposition in the aggregate, as well as the local environment of the matrix. Therefore, the complexity of CSF containing high concentrations of sodium, chloride, and magnesium ions introduces a gap of uncertainty in the optical response, consequently worsening the performance of Au@RR@AuNPs sensors when applied to real biofluids with respect to the simplified synthetic model of fluids.

Contrarily in the SERS-based approach, this limitation could be overcome considering that the configuration of the gold NPs, constituted by inner and outer layers of gold at fixed distances with an embedded Raman probe, guarantees high stability of the signal and strong repeatability of the measurements, which is not altered by changing conditions in the solution. Furthermore, the enhancement of the Raman signal was expected to be proportional to the collective effect of the particles participating in the aggregation, triggered uniquely by amyloid peptides that are in solution. The higher

https://doi.org/10.1021/acssensors.3c00225
ACS Sens. 2023, 8, 3693−3700

the amount of Aβ (1−42), the higher the number of NP−Aβ complexes aggregating, thus enhancing the cooperative effect and increasing the Raman signal proportionally. SERS spectra reported in Figure 6a successfully confirmed this hypothesis. Indeed, signals were characterized by Raman intensity @ 2135 cm^{-1}, increasing proportionally to the Aβ (1−42) quantity in the CSF batches. Plotting the Raman intensities as a function of the Aβ (1−42) concentration in the CSF samples (Figure 6b), data follows the trend previously identified with the synthetic model, with LOD values in the same pM range (Figure S10). This successful result was trivial, considering the enormous complexity of human fluids in terms of composition, pH, the presence of ions and salts, and proteins with respect to the Aβ synthetic model. Clearly, the uncertainty when working with real samples is higher with respect to synthetic models with no significant differences between concentrations. However, we then added a categorical scatterplot to attest that the NP sensors can consistently ($p < 0.0001$) distinguish two populations based on a Aβ (1−42) decisional threshold of 670 pg/mL (Figure S8). This value was quantified with standard clinical analytical methods (chemiluminescent enzyme immunoassay—CLEIA)[19] and is currently used, in combination with other AD biomarkers quantification. Moreover, TEM analyses of NP−Aβ (1−42) solution further attested the clustering behavior as a function of peptide concentration. At Aβ (1−42) lower concentrations, AuNPs mainly kept dispersed states of the original solution of NPs (Figure 6c) with the formation of aggregates composed of few particles, while at higher concentrations, larger aggregates composed of a higher number of particles consistently increase (Figures 6d,e and S9).

Even if the linearity range of NP-based sensors is lower with respect to the Aβ (1−40) content measured by standard kits (column 3 of table in Figure S7), to cross-check the specificity of the systems, the intensity of the Raman signals was plotted also against the concentration of Aβ (1−40). Reported data do not show a correlation with the analyte concentration, thus attesting that no quantification is possible for Aβ (1−40) (Figure S11).[11,20]

CONCLUSIONS

In conclusion, a novel rapid and low-cost optical assay for the detection of Aβ (1−42) was successfully developed by combining the simplicity of UV−vis detection with the sensitivity of the SERS method based on the bioorthogonal approach. This approach relies on the straightforward synthesis of novel multilayered SERS nanoprobes whose smart configuration, with bioorthogonal Raman reporters embedded within two layers of gold, enabled for fast revealing and quantification of Aβ (1−42) AD biomarkers with a sensitivity of pg/mL in highly complex human samples. Then, we demonstrated that the level of aggregation of NP−Aβ complexes could be simply modulated by the Aβ content itself and therefore proportionally reflected in the Raman intensity changes. Finally, based on these promising results, by switching the chemistry of NP surfaces, we envision the possibility to extend the Au@RR@AuNPs-based assay for the quantification of the other AD biomarkers (Aβ (1−40); protein Tau and phosphorylated Tau) as well as for the analysis of less-invasive biological fluids. Our pioneering approach based on bioorthogonal multilayered NPs represents a significant step ahead of the state of the art on SERS for biofluids analyses as well as a powerful contribution in the worldwide attempt to find more effective tools for the β amyloid-linked pathologies as Alzheimer' s disease diagnosis.

ASSOCIATED CONTENT

Supporting Information

The Supporting Information is available free of charge at https://pubs.acs.org/doi/10.1021/acssensors.3c00225.

Detailed materials and methodologies, characterization techniques, aggregation index explanation, and table resuming CSF samples (PDF)

AUTHOR INFORMATION

Corresponding Author

Caterina Credi − *European Laboratory for Non-Linear Spectroscopy (LENS), Sesto Fiorentino 50019, Italy; National Institute of Optics (INO), National Research Council (CNR), Sesto Fiorentino 50019, Italy;* orcid.org/0000-0003-4565-5214; Email: caterina.credi@ino.cnr.it, credi@lens.unifi.it

Authors

Caterina Dallari − *European Laboratory for Non-Linear Spectroscopy (LENS), Sesto Fiorentino 50019, Italy; Department of Physics, University of Florence, Sesto Fiorentino 50019, Italy; National Institute of Optics (INO), National Research Council (CNR), Sesto Fiorentino 50019, Italy*

Elena Lenci − *Department of Chemistry, University of Florence, Sesto Fiorentino 50019, Italy;* orcid.org/0000-0001-7408-2828

Andrea Trabocchi − *Department of Chemistry, University of Florence, Sesto Fiorentino 50019, Italy;* orcid.org/0000-0003-1774-9301

Valentina Bessi − *Department of Neurological and Psychiatric Sciences (NeuroFarba), University of Florence, Firenze 50134, Italy*

Silvia Bagnoli − *Department of Neurological and Psychiatric Sciences (NeuroFarba), University of Florence, Firenze 50134, Italy*

Benedetta Nacmias − *Department of Neurological and Psychiatric Sciences (NeuroFarba), University of Florence, Firenze 50134, Italy; IRCCS Fondazione Don Carlo Gnocchi, Firenze 50143, Italy*

Francesco Saverio Pavone − *European Laboratory for Non-Linear Spectroscopy (LENS), Sesto Fiorentino 50019, Italy; Department of Physics, University of Florence, Sesto Fiorentino 50019, Italy; National Institute of Optics (INO), National Research Council (CNR), Sesto Fiorentino 50019, Italy;* orcid.org/0000-0002-0675-3981

Complete contact information is available at: https://pubs.acs.org/10.1021/acssensors.3c00225

Author Contributions

The manuscript was written through contributions of all authors. All authors have given approval to the final version of the manuscript.

Notes

The authors declare no competing financial interest.

ACKNOWLEDGMENTS

This work was supported by DoptoScreen project (Fondo di Beneficenza Intesa San Paolo 2019, B/2019/0289) and RISE

project. The authors also wish to acknowledge Fulvio Ratto, Sonia Centi, and Roberto Pini (Institute of Applied Physics 'N. Carrara', CNR-Florence, Italy) for their assistance in the experiments. The authors would like also to thank the Centre for Electron Microscopies (Ce.ME) and the "Centro di competenza—RISE" funded by FAS Regione Toscana. This work was in part supported by the European Union's Horizon2020 research and innovation program under grant agreement no 871124 Laserlab-Europe.

REFERENCES

(1) Lutz, W.; Sanderson, W.; Scherbov, S. The Coming Acceleration of Global Population Ageing. *Nature* **2008**, *451*, 716−719.
(2) Braak, H.; Braak, E. Demonstration of Amyloid Deposits and Neurofibrillary Changes in Whole Brain Sections. *Brain Pathol.* **1991**, *1*, 213−216.
(3) Verdile, G.; Fuller, S.; Atwood, C. S.; Laws, S. M.; Gandy, S. E.; Martins, R. N. The Role of Beta Amyloid in Alzheimer's Disease: Still a Cause of Everything or the Only One Who Got Caught? *Pharmacol. Res.* **2004**, *50*, 397−409.
(4) Lassmann, H.; Bancher, C.; Breitschopf, H.; Wegiel, J.; Bobinski, M.; Jellinger, K.; Wisniewski, H. M. Cell Death in Alzheimer's Disease Evaluated by DNA Fragmentation in Situ. *Acta Neuropathol.* **1995**, *89*, 35−41.
(5) Gao, N.; Sun, H.; Dong, K.; Ren, J.; Duan, T.; Xu, C.; Qu, X. Transition-Metal-Substituted Polyoxometalate Derivatives as Functional Anti-Amyloid Agents for Alzheimer's Disease. *Nat. Commun.* **2014**, *5*, No. 3422.
(6) Forlenza, O. V.; Radanovic, M.; Talib, L. L.; Aprahamian, I.; Diniz, B. S.; Zetterberg, H.; Gattaz, W. F. Cerebrospinal Fluid Biomarkers in Alzheimer' s Disease: Diagnostic Accuracy and Prediction of Dementia. *Alzheimer's Dement.: Diagn. Assess. Dis. Monit.* **2015**, *1*, 455−463.
(7) d'Abramo, C.; d'Adamio, L.; Giliberto, L. Significance of Blood and Cerebrospinal Fluid Biomarkers for Alzheimer's Disease: Sensitivity, Specificity and Potential for Clinical Use. *J. Pers. Med.* **2020**, *10*, No. 116.
(8) Sehlin, D.; Englund, H.; Simu, B.; Karlsson, M.; Ingelsson, M.; Nikolajeff, F.; Lannfelt, L.; Pettersson, F. E. Large Aggregates Are the Major Soluble Aβ Species in AD Brain Fractionated with Density Gradient Ultracentrifugation. *PLoS One* **2012**, *7*, No. e32014.
(9) Lesné, S.; Kotilinek, L. Amyloid Plaques and Amyloid-β Oligomers: An Ongoing Debate. *J. Neurosci.* **2005**, *25*, 9319−9320.
(10) Zhou, Y.; Dong, H.; Liu, L.; Xu, M. Simple Colorimetric Detection of Amyloid β -Peptide (1 − 40) Based on Aggregation of Gold Nanoparticles in the Presence of Copper Ions. *Small* **2015**, *11*, 2144−2149.
(11) Yokoyama, K.; Welchons, D. R. The Conjugation of Amyloid Beta Protein on the Gold Colloidal Nanoparticles' Surfaces. *Nanotechnology* **2006**, *18*, No. 105101.
(12) Cheng, L.; Zhang, Z.; Zuo, D.; Zhu, W.; Zhang, J.; Zeng, Q.; Yang, D.; Li, M.; Zhao, Y. Ultrasensitive Detection of Serum MicroRNA Using Branched DNA-Based SERS Platform Combining Simultaneous Detection of α-Fetoprotein for Early Diagnosis of Liver Cancer. *ACS Appl. Mater. Interfaces* **2018**, *10*, 34869−34877.
(13) Zhu, W.; Wang, Y.; Xie, D.; Cheng, L.; Wang, P.; Zeng, Q.; Li, M.; Zhao, Y. In Situ Monitoring the Aggregation Dynamics of Amyloid-β Protein Aβ42 in Physiological Media via a Raman-Based Frequency Shift Method. *ACS Appl. Bio Mater.* **2018**, *1*, 814−824.
(14) Lin, L.; Tian, X.; Hong, S.; Dai, P.; You, Q.; Wang, R.; Feng, L.; Xie, C.; Tian, Z. Q.; Chen, X. A Bioorthogonal Raman Reporter Strategy for SERS Detection of Glycans on Live Cells. *Angew. Chem., Int. Ed.* **2013**, *52*, 7266−7271.
(15) Wang, J.; Liang, D.; Jin, Q.; Feng, J.; Tang, X. Bioorthogonal SERS Nanotags as a Precision Theranostic Platform for in Vivo SERS Imaging and Cancer Photothermal Therapy. *Bioconjugate Chem.* **2020**, *31*, 182−193.
(16) Dallari, C.; Innocenti, R.; Lenci, E.; Trabocchi, A.; Pavone, F. S.; Credi, C. Design and Synthesis of Novel Raman Reporters for Bioorthogonal SERS Nanoprobes Engineering. *Int. J. Mol. Sci.* **2022**, *23*, No. 5573.
(17) Bush, A. I. Drug Development Based on the Metals Hypothesis of Alzheimer's Disease. *J. Alzheimer's Dis.* **2008**, *15*, 223−240.
(18) Qiu, T.; Liu, Q.; Chen, Y. X.; Zhao, Y. F.; Li, Y. M. Aβ42 and Aβ40: Similarities and Differences. *J. Pept. Sci.* **2015**, *21*, 522−529.
(19) Zecca, C.; Brescia, V.; Piccininni, M.; Capozzo, R.; Barone, R.; Barulli, M. R.; Logroscino, G. Comparative Evaluation of Two Immunoassays for Cerebrospinal Fluid β-Amyloid 1−42 Measurement. *Clin. Chim. Acta* **2019**, *493*, 107−111.
(20) Jiang, D.; Rauda, I.; Han, S.; Chen, S.; Zhou, F. Aggregation Pathways of the Amyloid β(1 42) Peptide Depend on Its Colloidal Stability and Ordered β-Sheet Stacking. *Langmuir* **2012**, *28*, 12711−12721.

https://doi.org/10.1021/acssensors.3c00225
ACS Sens. 2023, 8, 3693−3700